

# Experimental partitioning of uranium between liquid iron sulfide and liquid silicate: Implications for radioactivity in the Earth's core

Kevin T. Wheeler <sup>a,\*</sup>, David Walker <sup>a</sup>, Yingwei Fei <sup>b</sup>, William G. Minarik <sup>c</sup>,  
William F. McDonough <sup>d</sup>

<sup>a</sup> Lamont Doherty Earth Observatory, Department of Earth and Environmental Sciences, Columbia University, Palisades, NY 10964, USA

<sup>b</sup> Geophysical Laboratory, Carnegie Institution of Washington, 5251 Broad Branch Road NW, Washington, DC 20015, USA

<sup>c</sup> Department of Earth and Environmental Sciences, McGill University, Montréal, Que., Canada H3A 2A7

<sup>d</sup> Department of Geology, University of Maryland, College Park, MD 20742, USA

Received 24 June 2005; accepted in revised form 17 November 2005

## Abstract

Measurable uranium (U) is found in metal sulfide liquids in equilibrium with molten silicate at conditions appropriate for a planetary magma ocean: 1–10 GPa, 1750–2100 °C, 0–28 wt% S, and  $f_{O_2}$  2 log units below IW. However, the transfer of U from metal sulfide to silicate under our experimental conditions is so complete that insufficient U would remain so as to be of any importance to the core's heat budget. U content in the sulfide phase increases strongly with S content but shows no significant variability with either pressure or temperature. Maximum  $D_{U}^{\text{sulfide/silicate}}$  is 0.001 while most values are considerably lower.

© 2006 Elsevier Inc. All rights reserved.

## 1. Introduction

The core's heat budget has an important influence on many major Earth processes. Generation of the Earth's geodynamo, the core's thermal evolution, formation of the inner core, and mantle convection are all processes that are intimately coupled to heat escape from the core. The source of the Earth's core's heat has long been a topic of keen interest, avid research, and spirited debate.

There are several plausible explanations for the heat escaping from the Earth's core. The simplest is that there is no current heat production and that the core-mantle boundary (CMB) heat flux of 6–12 TW (e.g., Buffett, 2003) is principally due to secular cooling. This scenario is inconsistent with most models of geodynamo power requirements coupled with Earth's thermal history and inner core formation age (Buffett, 2003). However, if there is moderate ohmic dissipation, the need for heat production

is reduced, making secular cooling a more plausible option (Christensen and Tilgner, 2004). The formation and accretion of the inner core provides an alternative source for heat generation. Fe metal freezing at the inner core boundary (ICB) from an Fe-alloy outer core causes latent heat of fusion to be released. Furthermore, loss of Fe decreases the density of the residual liquid alloy thereby increasing the alloy's gravitational potential energy that is converted partially to heat by viscous friction as it rises toward the CMB (e.g., Labrosse et al., 2001). Finally, any radioactive elements present in the Earth's core could produce heat.

A significant experimental and theoretical effort has attempted to establish the viability of K as a radioactive heat producer in the core. The Earth's major radioactive elements, K, U, and Th, are widely considered lithophile and therefore are not expected to partition into the Fe-alloy core. However, examination of carbonaceous chondrite versus bulk silicate Earth (BSE) abundances shows that K is depleted in the Earth by ~50%, while U and Th are slightly enriched (Palme and O'Neill, 2003; McDonough, 2003). This is not unexpected due to the volatile nature of K, though there is no isotopic evidence that

\* Corresponding author.

E-mail address: [kwheeler@ldeo.columbia.edu](mailto:kwheeler@ldeo.columbia.edu) (K.T. Wheeler).

K has experienced any considerable volatilization and evaporation (Humayun and Clayton, 1995). Thus, there is K absent from the silicate earth, and one place it could be sequestered is in the core. Hall and Murthy (1971) were early proponents of this hypothesis on thermodynamic grounds, followed by quantum mechanical calculations of Fe–K alloys (e.g., Bukowinski, 1976), diamond cell high pressure experiments (e.g., Lee and Jeanloz, 2003) and recent piston cylinder experiments (Murthy et al., 2003).

Though U and Th have received much less attention than K, there is evidence that they too may partially partition into the core. Herndon (1998) has long been a proponent of U in the core. Furthermore, the Th/U ratio of the BSE may be slightly different than that of chondrites. This could be consistent with up to 5 ppb U and 0.17 ppb Th in the core (Labrosse et al., 2001). Furthermore, studies of enstatite chondrites suggest that U and Th can trade their lithophile behavior for chalcophile behavior at very low  $f_{O_2}$  by partitioning into oldhamite (CaS) (Murrell and Burnett, 1982; Furst et al., 1982). Moreover, piston cylinder experiments of U and Th partitioning between liquid Fe–FeS and a variety of liquid silicate compositions suggest that U could prefer sulfide to silicate under the correct conditions (Murrell and Burnett, 1986). Additionally, a study of the “binary” system steel- $UO_2$  indicates that the immiscibility between the two ingredients decreases as a function of temperature and could ultimately disappear (Hodkin and Potter, 1980; Feber et al., 1984). The implication of all these studies is that the assumptions behind the conventional wisdom on U and Th partitioning may be incorrect and should be reexamined. It should be noted that evidence against U in the core exists too. Jones and Burnett (1980) found no appreciable U in the Fe-alloy of their 1 atmosphere silicate-FeSi and silicate-FeC partitioning experiments.

The purpose of this paper is to examine the plausibility of U as a heat producer in the Earth’s core by performing a series of U partitioning experiments conducted at conditions and compositions potentially applicable to the magma ocean of the early Earth. The sensitivity of plasma mass spectroscopy for U in metals makes the determination of U partitioning possible at the low abundance levels encountered.

## 2. Experimental methods

### 2.1. Starting material

Natural KLB-1, a fertile peridotite (Table 1), was combined with Fe and FeS to make starting compositions with roughly chondritic Fe/Si and different S contents (0, 7, and 28 wt% in the sulfide). S was chosen as the alloying component because it may be a light element in the core and because of previous suggestions that U may show chalcophile tendencies. KLB-1 powder was ground in an agate mortar under ethanol with various proportions of high purity, industrially prepared Fe and FeS powders. All mixtures

Table 1  
Comparison of KLB-1 compositions

	(a)	(b)	(c)
SiO <sub>2</sub>	44.48	44.30	44.82
TiO <sub>2</sub>	0.16	0.12	0.12
Al <sub>2</sub> O <sub>3</sub>	3.59	3.54	3.51
FeO <sup>a</sup>	8.10	8.59	7.30
MgO	39.22	39.50	39.90
CaO	3.44	3.03	2.97
Na <sub>2</sub> O	0.30	0.30	0.51

All values are weight percent. (a) Hirose and Kushiro (1993), (b) Herzberg et al. (1990), (c) This study: average from 8 analyses of MA811, a KLB-1-only multi anvil experiment run in a graphite capsule at 10 GPa and 2250 °C for 5 min. KLB-1 composition from this study is comparable to (a) and (b).

<sup>a</sup> All Fe as FeO.

were dried on a hotplate at low heat and stored in desiccating jars until use.

A U metal wire ( $^{238}U/^{235}U = 137.88$ ) was used as the U source. In most cases, a diamond file was used to shave small amounts of U from the wire. A thin, oxidized layer coated the wire; but the majority of U added to experiments was in metal rather than oxide form. The U metal was added to the KLB-1 + FeFeS mixture as a thin sprinkling near the middle of the sample capsule (Fig. 1). The U was not ground into the mixture in order to avoid contamination of the mortar and pestle.

### 2.2. Sample capsule

High-purity graphite (C) was machined to make capsules for both piston cylinder and multi-anvil experiments. Graphite was chosen primarily for its ability to limit oxygen fugacity. This is important as U is extremely easily oxidized. Some sample interaction with the capsule was observed in almost all runs (Fig. 2). C capsules were effective at containing their contents, though some contamination from the thermocouples was observed in several cases. The use of C capsules at high pressure (10 GPa) had the inconvenient drawback of occasional conversion to diamond.

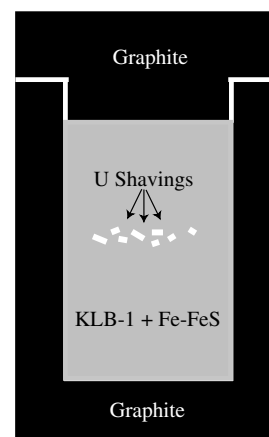


Fig. 1. Typical graphite capsule arrangement: inset lid covers KLB1 + FeFeS mixture with U metal shavings in the approximate middle.

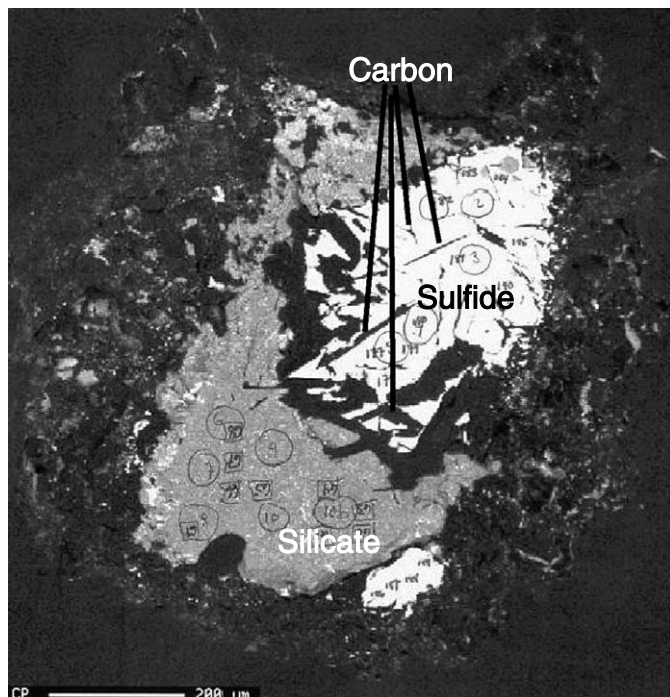


Fig. 2. BSE image of MA813, a multi anvil experiment at 10 GPa and 1950 °C. The bright material is FeFeS. The apparent large volume fraction of metal in this image is merely the consequence of this particular section through the charge. The light grey material is quenched silicate. The dark material is carbon. Carbon laths in the sulfide are evidence for interaction between the capsule and sample. Hand-drawn circles are approximate locations and sizes of LA-ICP-MS analyses. Smaller hand-drawn boxes and numbers are approximate locations and sizes of electron microprobe analyses.

### 2.3. Assemblies

#### 2.3.1. Talc–pyrex piston cylinder

The standard Geophysical Laboratory (GL) talc–pyrex piston cylinder assembly was used for 1–3 GPa and 1850–2100 °C experiments (Fig. 3). The graphite capsule was enclosed in an MgO cylinder sandwiched between two MgO spacers. To reduce void space, MgO powder was packed tightly around the capsule. The capsule and MgO slid into a graphite heater that was located within a talc–pyrex pressure media sleeve. The assembly was wrapped in lead foil before being inserted into the pressure vessel. A graphite end cap was placed at the bottom of the assembly and a steel plug was placed on top. A W-Re Type C thermocouple was housed in four-hole Al<sub>2</sub>O<sub>3</sub> tubing and slid through a pre-drilled hole in the steel plug and upper MgO spacer. Care was taken to place the thermocouple as close as possible to the capsule without puncturing it. Pressure in this assembly was friction corrected –10% based on Akella (1973).

#### 2.3.2. BaCO<sub>3</sub>–LaCrO<sub>3</sub> piston cylinder

The BaCO<sub>3</sub>–LaCrO<sub>3</sub> assembly (Cottrell and Walker, 2006) employed a LaCrO<sub>3</sub> sleeve as a thermal insulator and BaCO<sub>3</sub> as the pressure medium (Fig. 4). This design allows for run durations of 30 min or more at temperatures

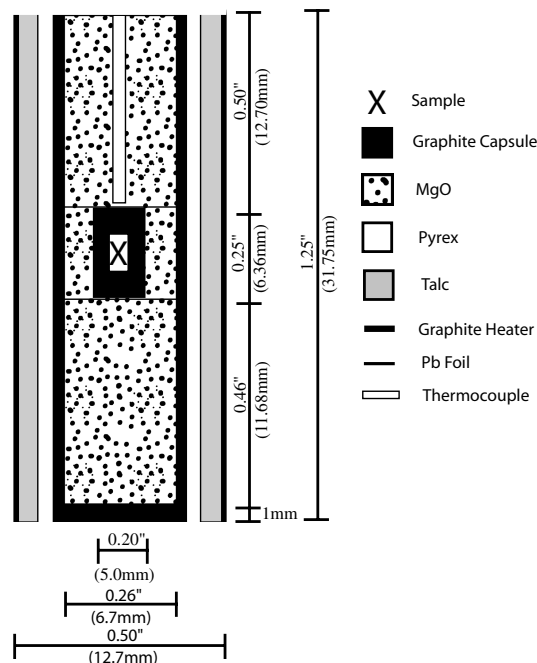


Fig. 3. Standard Geophysical Lab talc–pyrex piston cylinder assembly (Kushiro, 1976).

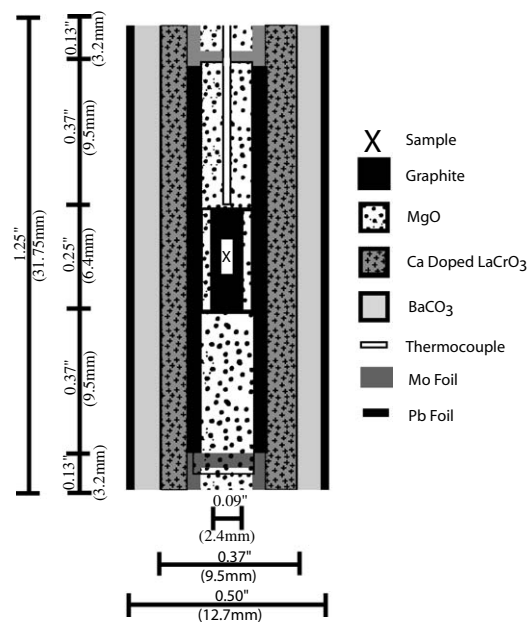


Fig. 4. High T 1/2 in. piston cylinder assembly.

up to 2500 °C and pressures of 1–2 GPa. It was used for one high temperature (2300 °C) experiment in this study.

#### 2.3.3. Multi-anvil

A cubic/octahedral multi-anvil pressurization device with Toshiba Grade F tungsten carbide cubes with 5 mm truncated edge lengths was used for experiments at 10 GPa (Fig. 5). Graphite capsules were placed inside an MgO sleeve that was plugged at both ends by Al<sub>2</sub>O<sub>3</sub> spac-

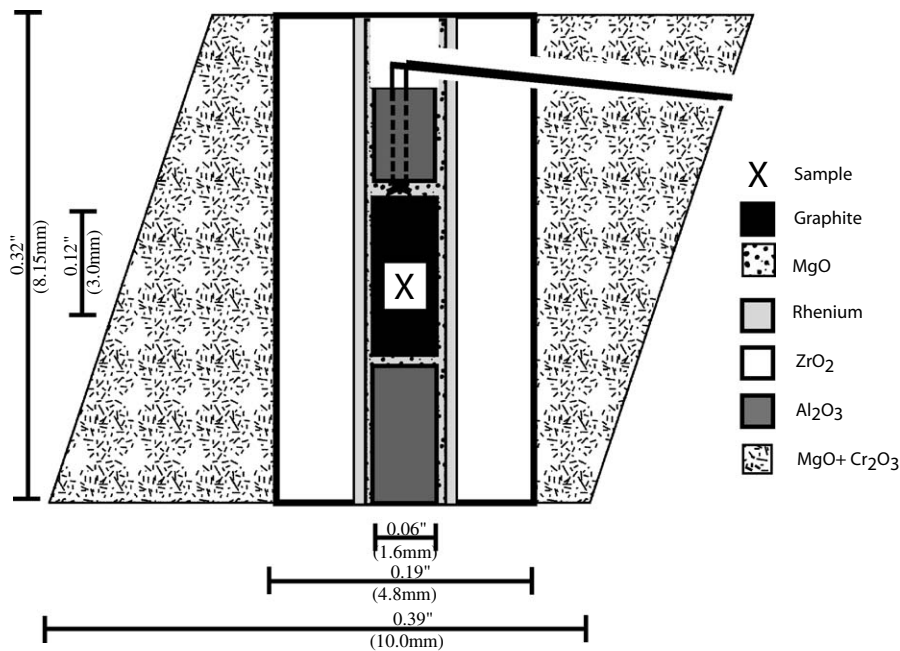


Fig. 5. 10/5 multi-anvil assembly.

ers. The upper spacer housed the W-Re Type C thermocouple and was separated from the capsule by a thin layer of MgO powder. The MgO sleeve was placed in a 0.0025 in. thick Re heater that was itself enclosed in a ZrO<sub>2</sub> thermal insulator. This ensemble was housed in a 10/5 MgO + Cr<sub>2</sub>O<sub>3</sub> (5 wt%) octahedron. Grooves for the thermocouple leads were cut in the MgO by hand. ZrO<sub>2</sub> cement was used to secure the thermocouple in the octahedra and to fill in any void spaces. Pressure calibration is described by Bertka and Fei (1997).

## 2.4. Procedure

### 2.4.1. Capsule loading

KLB-1 + FeFeS powder was placed into graphite capsules with a platinum wire scraper. The powder was packed with a tungsten-carbide drill blank. Once the capsule was approximately half full, U metal shavings were added, followed by another layer of KLB-1 + FeFeS powder. All contents were then packed again and covered by a graphite lid. The capsule was loaded into a sample assembly which was either run immediately or stored in a dry box. It was not possible to do a U mass balance for these experiments because the quantity of U metal added to each experiment was too small to be measured accurately on a balance. However, analyzed metal and silicate phases in run products indicate that the quantity of U remaining in the charge after each run was on the order of 1 wt%. There was no U leakage or mobilization witnessed in the area surrounding the capsule.

### 2.4.2. Piston cylinder

Most talc-pyrex runs were conducted in a 250 ton Boyd-England style apparatus. They were brought directly to P

and T without a sintering step. Run durations were 20–205 min. Quenching was performed by turning off the power to the heater. Decompression was completed quickly by opening the pressure-ram valve. The BaCO<sub>3</sub>–LaCrO<sub>3</sub> run included an additional sintering step at 800 °C for 12–24 h.

### 2.4.3. Multi-anvil

Runs were conducted in a 800 ton Walker-style apparatus. They were typically pressurized at 50 bars/h, and reached 10 GPa at ~180 tons and 320 bars. A sintering step at 800 °C, 10 GPa for approximately three hours was commonly included. Run durations ranged from 1 to 20 min. The transformation from the initial small grain size and thorough mixture of the metal and silicate phases into coarse segregations of liquid metal and liquid silicate indicates chemical reorganization on the scale of the charge. Equilibrium was judged as likely to have been reached based on the textural evolution observed and on the diffusion length scales in molten materials at these conditions (Walker and Agee, 1989). Quenching was accomplished by turning off the power to the heater. Runs were typically decompressed from 320 bars to 1 atmosphere at 50 bars/h. Sample run summaries can be seen in Table 2.

## 2.5. Sample preparation and polishing

### 2.5.1. Piston cylinder

The sample assemblies and/or the graphite capsules were placed in epoxy and cured for several hours. A diamond wheel and silicon carbide paper were used with water to grind into the sample. A lapidary wheel with 1 μm diamond paste or 0.3 μm Al<sub>2</sub>O<sub>3</sub> grit was used to impart the final polish. A typical run product can be seen in Fig. 6.

Table 2  
Run conditions, starting materials, and partition coefficients

Run	Sulfide	P (Gpa)	T (°C)	Time (min)	$\log(O_2/\Delta IW)$	$D_{Ni}^{sulfide/silicate}$	$D_{Co}^{sulfide/silicate}$	$D_{Ni}^{sulfide/silicate}$	$D_{W}^{sulfide/silicate}$	$D_{U}^{sulfide/silicate}$										
<i>Piston cylinder</i>																				
PC405	Fe–FeS 7%	2	2100	26	–2.06	0.014	0.008	0.006	104.04	30	20	295	34	28	105	138	95	3.3E–05	3.6E–05	2.3E–05
PC408	Fe metal only	2	1850	110	–2.02	0.024	0.005	0.004	157.56	26	22	657	140	98	31	19	10	1.7E–05	1.1E–05	3.0E–06
PC409	Fe–FeS 28%	2	1850	20	–2.23	0.120	0.032	0.031	232.47	—	—	—	—	—	14	8	5	4.1E–04	8.8E–05	8.0E–05
PC412	Fe–FeS 7%	2	1750	205	–2.02	0.014	0.003	0.002	106.82	23	18	347	512	130	26	7	5	0.0E+00	—	—
PC413	Fe–FeS 7%	3	1850	74	–2.31	0.010	0.001	0.001	—	—	—	339	43	34	5	3	1	2.4E–05	1.6E–05	1.5E–05
GG922	Fe metal only	1	2300	6	–2.02	—	—	—	—	—	—	—	—	—	—	—	—	0.0E+00	—	—
<i>Multi-anvil</i>																				
MA802	Fe–FeS 28%	10	2000	20	–1.92	0.205	0.054	0.054	93.122	5	5	502	90	66	14	4	3	1.2E–03	2.9E–05	2.3E–05
MA805	Fe–FeS 28%	10	1850	20	–1.80	0.345	0.058	0.057	77.507	11	9	206	7	6	8	1	1	8.7E–04	1.5E–05	9.6E–06
MA813	Fe–FeS 7%	10	1950	1	–1.98	0.130	0.028	0.027	95.643	15	12	423	64	49	6	9	3	1.9E–05	9.2E–06	8.6E–06
MA819	Fe–FeS 28%	10	1800	5	–1.83	0.203	0.044	0.039	—	—	—	—	—	—	8	6	3	8.2E–04	3.3E–04	2.7E–04

Calculation of partition coefficients and their errors is described in the text. Oxygen fugacity is calculated relative to the IW buffer:  $\Delta IW = 2^* \log(a_{FeO}/a_{Fe})$  where activities are estimated as mole fractions.

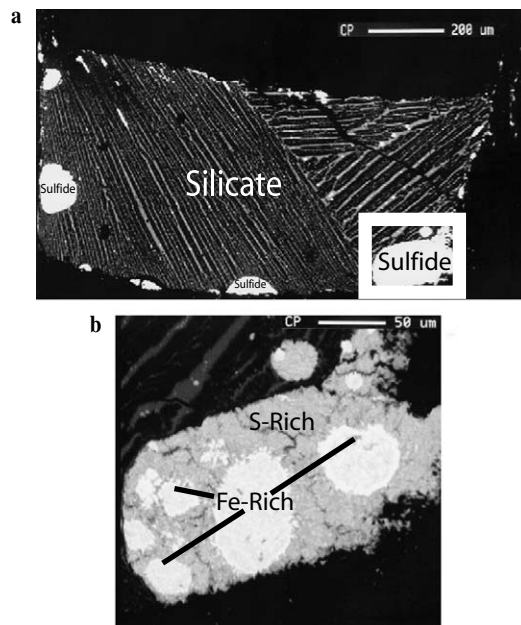


Fig. 6. BSE image of PC409. At P and T, silicate and sulfide were assumed molten and homogenous. Upon quench, characteristic textures developed in the silicate and metal/sulfide. (a) Quenched silicate melt developed spinifex texture with olivine laths cutting through residual Ca-, Al-, and U-rich residual glass. (b) Quenched sulfide melt resulted in metal and sulfide segregation. This effect was witnessed more strongly in the piston cylinder experiments which had a slower quench rate than the multi-anvil.

### 2.5.2. Multi-anvil

The conversion of graphite capsules to diamond complicated post-run sample preparation. Sectioned octahedra were placed in epoxy and cured in a 100 °C oven for several hours. A series of diamond wheels were used with water to grind into the capsule. Final polishing was done with a series of 15–9 μm diamond paper and 1 μm diamond paste on a lapidary wheel. The multi-anvil run polishing was plagued by differences in hardness between the diamond capsule and the silicate. Furthermore, severe plucking posed a problem. Careful polishing with the diamond paper succeeded in alleviating these problems in most samples.

## 3. Analysis

### 3.1. Electron microprobe

Experiments were analyzed on the Carnegie Institution of Washington Geophysical Lab's JEOL 8900 electron microprobe. Sulfide and metal were analyzed with a 15 kV accelerating voltage and a 50 nA sample current. Elements were analyzed with 30 s count times for peaks and 15 s count times for backgrounds. Fe(Kα) and S(Kα) were standardized with pyrite, Ni(Kα) with NiS and U(Mβ) with pure, industrially prepared metal. Silicates were analyzed with 15 kV accelerating voltage and a 20 nA sample current. Na(Kα), Mg(Kα), Al(Kα), Si(Kα), Ca(Kα), Ti(Kα), and Fe(Kα) were standardized with basalt glass. U(Mα) was standardized with UO<sub>2</sub>. As both the sil-

icate and the metallic phase quenched heterogeneously (Fig. 6), raster mode analyses were made to capture the ‘average’ composition. Typical raster magnifications produced fields of view from 100 to 300  $\mu^2$ . A standard ZAF correction was applied to all data.

A U-free iron sulfide was used to check the U background in the sulfide. It was found that the background in the sulfide was too high to reliably detect U. However, the high, weight percent level, U concentrations in the silicate allowed for accurate measurement with the electron microprobe.

### 3.2. LA-ICP-MS

The laser ablation inductively coupled plasma mass spectrometer (LA-ICP-MS) was used to detect U as well as other trace elements in both the metal-alloy and in the silicate. The facility at McGill University was used for all analyses mentioned in this study except experiment GG922.

#### 3.2.1. McGill university LA-ICP-MS

A Nd:YAG New-Wave UP-213 Laser Ablation System with a wavelength of 213 nm and an energy density of about 6 J/cm<sup>2</sup> was coupled to a Perkin-Elmer/SCIEX ELAN 6100 DRC plus ICP-MS. The ablation cell was continuously flushed with He gas for sensitivity enhancement. Most spot sizes were 30  $\mu\text{m}$  with a 5 Hz repetition rate.

All points were pre-ablated to insure a clean ablation surface. Characteristic measurements involved  $\sim 30$  s of background acquisition before  $\sim 50$  s of sample ablation. Collection times were shorter if the target was small and quickly ablated away. Two to six measurements were made per phase in each experiment depending on exposure area. The system was flushed with He for several minutes between silicate and sulfide measurements to reduce the high residual U background left over from the silicate ablation.

A series of primary and secondary standard measurements were made throughout the analyses to insure data reliability. Primary standards were typically run every four to six analyses. Secondary standards were usually run at the beginning and end of each sample’s analysis. NIST612 was used as the standard for the sulfide and metal while NIST610 (Pearce et al., 1997) was used for the silicate. The choice of primary standards was made based on trace element concentration. A Columbia River basalt (BCR2) (Ila and Frey, 2000) and a Hawaiian volcanic glass (BHVO) (Eggins et al., 1998) were used as secondary standards. A Chinese standard, GSR1 (Govindaraju, 1994), with a natural <sup>238</sup>U/<sup>235</sup>U ratio was used to test for isotopic fractionation in the machine. Ni data from the electron microprobe were used as the internal standard for the metal and sulfide. KLB-1 silicon data from the electron microprobe were used as the internal standard for the silicate.

All data were processed off line with GLITTER LA-ICP-MS processing software (GEMOC, Macquarie University,

Australia). The phase regions interpreted as silicate liquid or metal liquid blobs at the experimental P-T in the charges were heterogeneous mixtures of phases after capsule recovery. These mixtures are partly quench growths and partly dispersed mixtures of the primary silicate and metal liquids. A silicate phase was observed in the metal–sulfide and small sulfide blebs were observed in the silicate. Care was taken to ensure signal selection for each analysis represented ablation of either a pure metal–sulfide phase or a pure silicate phase. High Ni values in the silicate signal indicated the presence of equilibrium metal or sulfide, while high values of Al in the metal and sulfide indicated the presence of silicate. Ni and Al ‘contaminants’ were manifested as distinct sharp increases in intensity and were therefore interpreted to be heterogeneous regions. Sections of analyses that contained contaminants were discarded. The silicate contained numerous small metallic blebs that were interpreted as quench exsolutions from the liquid. These blebs contained no Ni detectable by microprobe and were therefore not responsible for the sharp Ni increases.

Background for most of the trace elements including U was essentially zero. For this reason, any counts at all were significant. The low background allowed for reliable detection of trace elements present at the 100 s of ppb level.

#### 3.2.2. University of Maryland LA-ICP-MS

A Nd:YAG New-Wave UP-213 Laser Ablation System was coupled to a Finnigan Element2 single collector ICP-MS. Most spot sizes were 15–30  $\mu\text{m}$  with a 7 Hz repetition rate. Power was similar to that used at McGill. Three to four analyses were made per phase. NIST610 was used as the standard for both the metal and silicate analyses. Ni data acquired from the electron microprobe were used as the internal standards for the metal phases while Ca data were used for the silicate. The metal phase was not physically thick so the laser quickly ablated through it. Therefore, peaks were on the order of only 10 s. Data were processed off line with Lamtrace software.

### 3.3. D value calculation and error

Silicate U concentrations from the microprobe were used with sulfide U concentrations from the LA-ICP-MS to calculate U’s partition coefficient between sulfide and silicate ( $D_{\text{U}}^{\text{sulfide/silicate}}$ ). The large analytical areas ( $\sim 700 \mu\text{m}^2$  for LA-ICP-MS,  $\sim 300 \mu\text{m}^2$  for electron microprobe) effectively averaged regions of the heterogeneous quench textures of much smaller scale. Bulk compositions of the silicate and sulfide phases were determined by averaging analyses taken on the respective phases. As these analyses represent local averages, uncertainty is best defined by the standard error of the mean (SEM):  $\sigma/\sqrt{n}$  where  $\sigma$  is the standard deviation of the large-area measurements and  $n$  is the number of analyses.  $D_{\text{U}}^{\text{sulfide/silicate}}$  was defined as the weight concentration of U in the bulk metal sulfide ( $C_{\text{U}}^{\text{sulfide}}$ ) phase divided by the concentration in the bulk silicate ( $C_{\text{U}}^{\text{silicate}}$ ). Upper error bounds were defined as  $(C_{\text{U}}^{\text{sulfide}} + \text{SEM}_{\text{U}}^{\text{sulfide}})/(C_{\text{U}}^{\text{silicate}} - \text{SEM}_{\text{U}}^{\text{silicate}})$ .

Table 3

(a) Average weight percent compositions of metal phases measured by EMP and LA-ICP-MS, (b) average weight percent major element oxide composition of silicate phases measured by EMP, (c) average weight percent minor element composition of silicate phases measured by LA-ICP-MS

	Fe	SEM S	SEM	Ni	SEM	Mn	SEM	Co	SEM W	SEM	U	SEM	Total						
<b>a</b>																			
<i>Piston cylinder</i>																			
PC405	92.5	2.6	2.4	2.5	0.21	0.01	0.001	0.000	0.027	0.001	1.5942	1.4116	0.00010	0.00005	96.75				
PC408	92.9	0.1	0.1	0.0	0.67	0.01	0.002	0.000	0.039	0.003	0.0103	0.0011	0.00002	0.00001	93.75				
PC409	75.3	2.6	21.4	2.8	0.69	0.05	0.009	0.002	0.031	0.004	0.0009	0.0003	0.00065	0.00010	97.45				
PC412	91.2	2.4	3.5	2.7	0.66	0.04	0.001	0.000	0.036	0.002	0.0155	0.0010	0.00000	—	95.47				
PC413	85.9	2.4	9.3	2.7	0.45	0.02	0.001	0.000	0.027	0.001	0.0002	0.0000	0.00004	0.00003	95.6				
<i>Multi-anvil</i>																			
MA802	69.3	0.6	28.8	0.7	0.46	0.03	0.017	0.004	0.028	0.001	0.0572	0.0076	0.00370	0.00203	98.59				
MA805	67.2	0.9	29.3	0.5	0.52	0.06	0.033	0.005	0.029	0.001	0.2143	0.0165	0.00531	0.00057	97.27				
MA813	87.8	0.2	6.8	0.2	0.52	0.03	0.011	0.002	0.035	0.001	0.0003	0.0001	0.00005	0.00002	95.15				
MA819	70.9	0.4	27.7	0.3	0.46	0.01	0.022	0.003	0.027	0.001	0.0023	0.0002	0.00206	0.00048	99.08				
	Na <sub>2</sub> O	SEM	TiO <sub>2</sub>	SEM	Al <sub>2</sub> O <sub>3</sub>	SEM	FeO	SEM	SO <sub>3</sub>	SEM	MgO	SEM	SiO <sub>2</sub>	SEM	UO <sub>2</sub>	SEM	CaO	SEM	Total
<b>b</b>																			
<i>Piston cylinder</i>																			
PC405	0.531	0.153	0.124	0.020	3.6	1.0	9.35	0.73	1.37	0.62	36.9	3.0	39.5	0.7	1.5	0.7	2.984	0.597	95.876
PC408	0.727	0.201	0.143	0.008	4.1	1.0	9.06	0.51	0.07	0.02	38.6	3.9	42.7	0.4	1.1	0.4	3.853	1.013	100.31
PC409	0.471	0.023	0.115	0.005	3.9	0.1	5.77	0.20	0.60	0.09	41.6	0.4	41.8	0.1	1.8	0.1	2.868	0.102	99.014
PC412	0.688	0.070	0.137	0.009	3.9	0.4	8.91	0.21	0.35	0.05	38.8	1.3	40.1	0.1	2.0	0.2	3.963	0.348	98.866
PC413	0.422	0.022	0.112	0.005	3.6	0.2	6.01	0.29	0.32	0.09	39.6	0.9	42.7	0.3	2.0	0.1	2.956	0.141	97.705
<i>Multi-anvil</i>																			
MA802	0.292	0.004	0.104	0.003	2.1	0.0	7.58	0.03	0.20	0.01	42.2	0.1	41.9	0.0	3.6	0.1	2.312	0.031	100.31
MA805	0.518	0.004	0.133	0.001	4.7	0.0	8.50	0.04	0.56	0.00	32.3	0.1	42.8	0.1	8.3	0.0	3.755	0.002	101.5
MA813	0.397	0.010	0.114	0.007	3.4	0.1	8.96	0.84	0.66	0.11	41.0	0.3	42.0	0.4	2.8	0.1	2.889	0.069	102.2
MA819	0.796	0.022	0.158	0.007	5.1	0.1	8.61	0.20	0.73	0.06	31.5	0.3	44.3	0.2	2.8	0.2	4.152	0.066	98.307
	Mn	SEM	Co	SEM	Ni	SEM	W	SEM											
<b>c</b>																			
<i>Piston cylinder</i>																			
PC405	0.066	0.008	0.00026	0.00005	0.0016	0.0002	0.0152	0.0028											
PC408	0.084	0.003	0.00025	0.00002	0.0010	0.0002	0.0003	0.0001											
PC409	0.085	0.002	0.00013	—	—	—	0.0001	0.0000											
PC412	0.093	0.004	0.00034	0.00004	0.0018	0.0011	0.0006	0.0001											
PC413	0.095	0.001	—	—	0.0012	0.0001	0.0000	0.0000											
<i>Multi-anvil</i>																			
MA802	0.084	0.001	0.00030	0.00000	0.0009	0.0001	0.0042	0.0004											
MA805	0.095	0.001	0.00037	0.00004	0.0025	0.0001	0.0273	0.0011											
MA813	0.088	0.001	0.00036	0.00004	0.0016	0.0002	0.0001	0.0000											
MA819	0.106	0.007	—	0.00020	—	0.0044	0.0003	0.0001											

Errors are calculated as standard error of the mean as described in text.

Lower error bounds were defined as  $(C_U^{\text{sulfide}} - \text{SEM}_U^{\text{sulfide}}) / (C_U^{\text{silicate}} + \text{SEM}_U^{\text{silicate}})$  (Jana and Walker, 1998). The  $D_s$  calculated in this study are in Table 2. The sulfide and silicate measurements are reported in Table 3.

## 4. Results

### 4.1. Run products

The initial mixture of KLB-1 and FeFeS separated under run conditions into a molten silicate-rich phase and a molten metal-rich phase. The silicate phase always dominated volumetrically. The metal phase tended to form round blobs that congregated on the graphite (or diamond) capsule walls due to favorable surface energy.

Upon quench, these phases acquired a new degree of complexity. The silicate liquid always quenched to a spinifex textured arrangement of Mg-rich olivine laths with Ca and Al-rich liquid between them. This texture was coarsest in lower pressure runs that quenched more slowly but was also present in the faster quenching, high pressure runs (Figs. 2 and 6). A further level of complexity was introduced by the presence of small (~1–5 μm) metallic blebs in the Ca Al zones of the quenched silicate. These metallic blebs are interpreted as exsolution from the silicate rather than as equilibrium metal at run conditions. Blebs from experiments in the same system but doped with Pd showed no detectable Pd from electron microprobe analyses while the large metal phases in the same experiments had high concentrations of Pd. This suggests that the small metal

blebs exsolved from the Pd-poor silicate. In the present study, the blebs in silicate showed no Ni to the electron probe. Therefore, when the mass spectrometer encountered sustained high Ni signals from what is supposed to be clean silicate, we interpreted those portions as having encountered the edges or tops of buried masses of equilibrium metal blebs and excluded them.

This situation has parallels to the metal blebs in silicate encountered by Cottrell and Walker (2006) in their study of Pt partitioning between metal and silicate. The textural evidence for non-growth of such small blebs in the fastest-cooled margins of quenched charges makes the quench-growth interpretation of blebs in the Pt-based study more obvious than here. However, this complication is of much less consequence for U partitioning because essentially no U enters the metal anyway, so inclusion or absence of these blobs in the analysis of the silicate makes no difference to  $D_U$ .

The presence of the occasional silicate blob within the analyzed metal masses or the sampling of silicate matrix surrounding or beneath the metal would have a very large impact upon  $D_U$ . Our careful exclusion of Al-contaminated signals from metal analyses, as representing dispersed silicate contaminant, not exsolved silicate, is perhaps a key to our significantly lower values for  $D_U$  than reported by previous workers.

The metal liquid also displays further complexity. Particularly in S-rich experiments, the metal is segregated into Fe-rich and S-rich areas (Fig. 6b). The experiments were conducted well above the Fe–FeS liquidus. Therefore, the two metallic phases may have been formed upon quench with locally concentrated crystallization of Fe from the sulfide liquid. It is also possible that there are two stable metallic liquids at high S content, one of which is C-rich.

#### 4.2. Partition coefficients

$D_U^{\text{sulfide/silicate}}$  is small (Table 2). The largest  $D_U^{\text{sulfide/silicate}}$  observed is approximately 0.001 which plainly shows that U is extremely incompatible in sulfide and partitions heavily into silicate. However, against this starkly lithophile backdrop, an interesting pattern of U partitioning behavior is detectable.

Regardless of P variation or S content,  $D_U^{\text{sulfide/silicate}}$  varies little with temperature (Fig. 7a).  $D_U^{\text{sulfide/silicate}}$  does not change appreciably in Fe metal at 1–2 GPa from 1850 to 2300 °C nor does it change between 1750 and 2100 °C in experiments with 7% S in the metal phase at 1 GPa. Experiments that contained 28 wt% S at 10 GPa similarly show no discernable temperature trend.

Pressure does not seem to significantly affect  $D_U^{\text{sulfide/silicate}}$  either (Fig. 7b). A 7 GPa pressure increase yields no change in  $D_U^{\text{sulfide/silicate}}$ . While the pressures of these experiments are fairly limited with respect to those present in the Earth, the trend observed in this data suggests that pressure may not be an important factor in variation of  $D_U^{\text{sulfide/silicate}}$ .

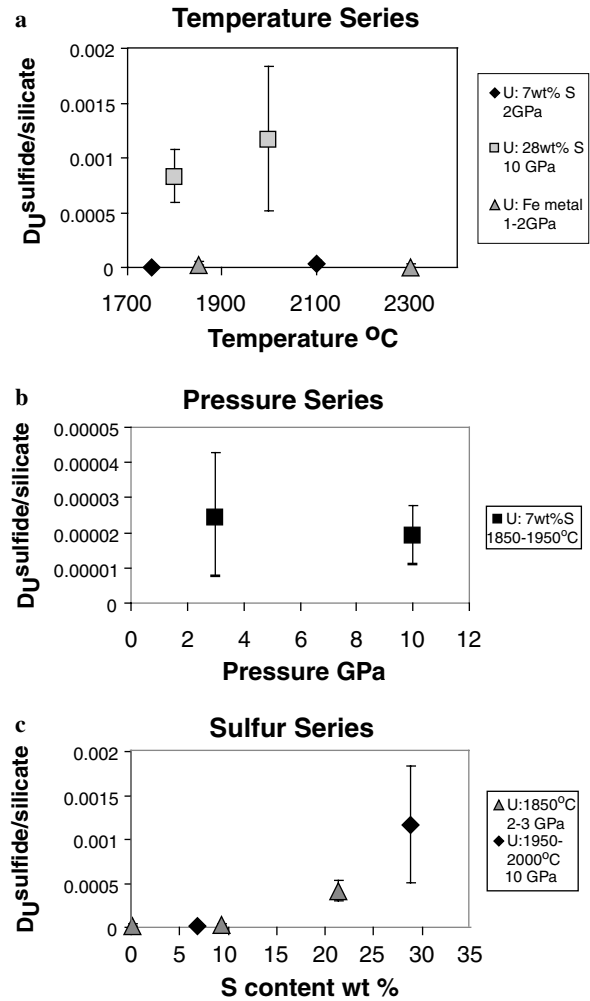


Fig. 7. (a–c) Plots of  $D_U^{\text{sulfide/silicate}}$  with respect to temperature, pressure, and S composition. Points that plot directly on the zero line had levels of U in the metal that were below approximate 0.3 ppm detection limits.

S composition seems to be the largest controlling factor of  $D_U^{\text{sulfide/silicate}}$  explored in this study (Fig. 7c). Sulfide in runs with low S contents contains little U while experiments with S contents of 20 wt% or higher have  $D_U^{\text{sulfide/silicate}}$  at least an order of magnitude larger. Low pressure, low temperature runs suggest the same S dependence as those at high pressure and moderate temperature.  $D_U^{\text{sulfide/silicate}}$  does not show variation with S content until 10–20 wt% S in the metal. This could be due to a logarithmic dependence of  $D_U^{\text{sulfide/silicate}}$  with S content.

The partition coefficients of several other elements were determined with respect to pressure, temperature and S composition. These elements were not added purposefully and either were originally present in KLB-1 or came from outside contamination such as W from the W-Re thermocouple. As published U partitioning data are sparse, these additional data provide a means by which to compare this study with others. Most of these elements show little variation in  $D_M^{\text{sulfide/silicate}}$  with any variable (Fig. 8). Mn is an exception which shows some responsiveness to pressure

(Fig. 8b) and some variation with respect to S content (Fig. 8c).

One detail which may strike the reader as odd is that there is no pressure effect on  $D_{Ni}^{\text{sulfide/silicate}}$  in our data. Several other studies have observed a significant negative pressure effect for Ni (e.g., Li and Agee, 2001; Chabot et al., 2005). One possible explanation for this discrepancy may be that our experiments contained less than one weight percent Ni while most others contained as much as an order of magnitude more. Our low pressure experiments return values for  $D_{Ni}$  very compatible with other studies at high Ni concentration,  $\sim 300$ , suggesting that our experiments are not completely divorced from the reality of these precedents, and that Henry's Law has not been violated at low pressure. However, there is no guarantee that Henry's Law will have the same constant at the full range of pressures and concentrations encountered.

The partition coefficients for U may be plotted against the regression parameter,  $-\ln(1 - 2\alpha X(S))$ , introduced by Jones and Malvin (1990). Fig. 9 uses the generic  $\alpha = 1.09$  that is best suited for a Fe–S matrix even though it is not

the silicate matrix encountered in this study. All data from this study, at all S abundances, are plotted regardless of pressure or temperature. That the elements plot in a linear fashion in Fig. 9 is consistent to a first order with Jones–Malvin S-avoidance behavior and is a validation of the approach, not of the specific choice of  $\alpha = 1.09$ . Alternatively, close examination of the low-S region of the U data might lead an examiner to conclude that the U plot has two different slopes, one at low S contents and another at higher S contents. This could suggest increasing chalcophile behavior for U once a certain threshold S value is reached; similar behavior is seen in Fig. 8c for Mn. Mn also exhibits chalcophile behavior in Fig. 9.  $D_{Mn}^{\text{sulfide/silicate}}$  increases gradually with S content and agrees well with data from Chabot and Agee (2003) in a similar system. Linear behavior on the Jones–Malvin plot suggests that S content influences  $D_M^{\text{sulfide/silicate}}$  more than any other variable investigated. Ni and Co show little observable variation with S content in marked contrast to the results of Jones and Malvin (1990) where they proved considerably chalcophobic. Jones and Malvin (1990) conducted their study in the liquid metal–solid metal system while this study is for partitioning between liquid metal sulfide and silicate. Reluctance of Ni and Co to leave the sulfide phase as the S content increases may be more indicative of their

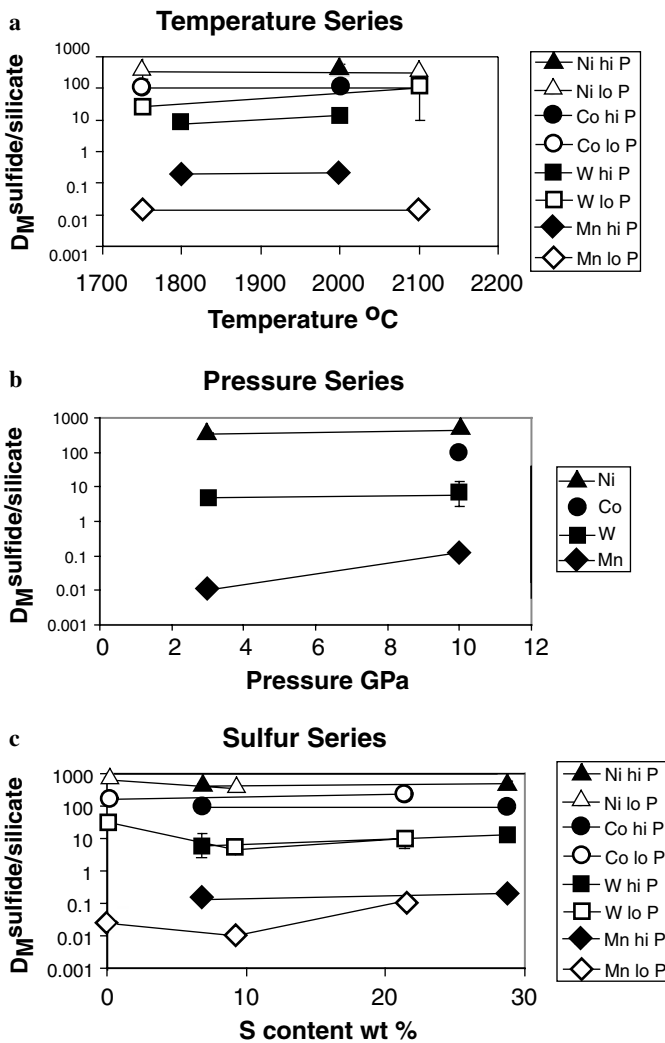


Fig. 8. (a–c) Plots of  $D_M^{\text{sulfide/silicate}}$  with respect to T, P, and S composition for various incidental elements.

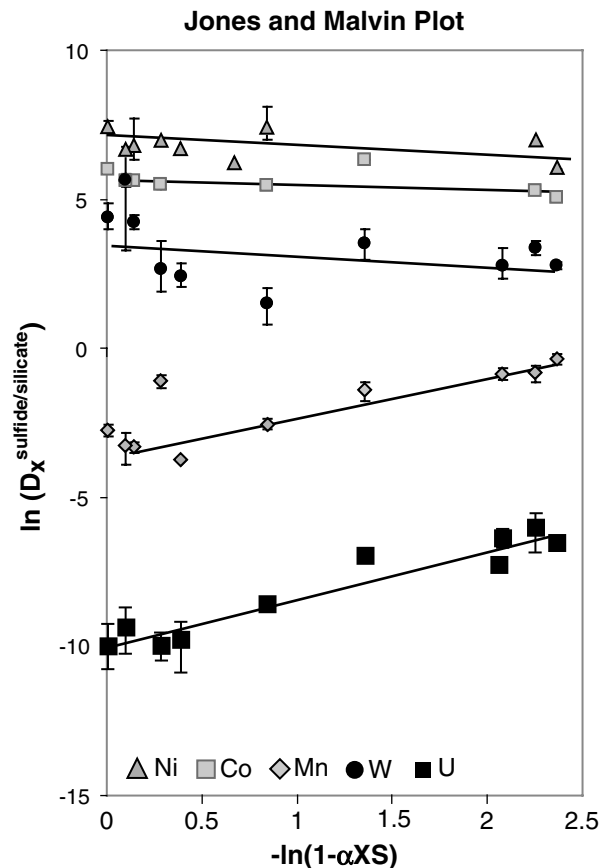


Fig. 9. The Jones and Malvin plot for U and incidental elements.

incompatibility in the silicate (aversion to oxygen) rather than their response to sulfur. W behaves similarly to Ni and Co in that it shows little variation with S content. This result is in contrast to published data from Jones and Malvin (1990) and Liu and Fleet (2001) for possibly the same reason as Ni and Co. Jana and Walker (1997) studied  $D_{\text{Ni}}^{\text{sulfide/silicate}}$  with varying S content and observed similar flat trends as seen in this study. That U and Mn do show an S-based response in our system becomes more significant in comparison to Ni, Co, and W.

## 5. Discussion

Consistent with the results from Jones and Burnett (1980), this study unambiguously shows that U remains exceptionally lithophile for conditions up to 10 GPa, 2300 °C and 28 wt% S. For this reason, to the extent that these conditions faithfully represent those of core formation, it is neither likely that U entered the core nor probable that it plays a large role in its heat production, especially if the core formed from an Earth with  $fO_2$  high enough for stable FeO to exist in the mantle. Calculations based on the energy of U decay indicate that for it to account for even 10% of the lower estimate of the core's heat budget, it would have to be present in concentrations of ~3 ppb. Assuming  $2.8\times$  CI chondritic original mantle abundances of refractory lithophile elements, a  $D_{\text{U}}^{\text{sulfide/silicate}}$  of almost 0.1 would be needed to account for this concentration. The maximum  $D_{\text{U}}^{\text{sulfide/silicate}}$  from this study is only ~0.001, much too low for U to be a significant heat producer in the core.

The findings of this study conflict with the study by Murrell and Burnett (1986). They conducted a series of piston cylinder experiments looking at U partitioning between FeFeS and silicate liquids of different compositions. They found a maximum  $D_{\text{U}}^{\text{sulfide/silicate}} > 1$  and a strong correlation between U and Ca concentrations in a system with basalt as the silicate. Experiments carried out with granite as the silicate yielded much lower  $D_{\text{U}}^{\text{sulfide/silicate}}$  of ~0.02. We looked for correlation between Ca and U in our experiments and did not find any. Even more, we did not observe the different Ca- and Al-rich phases in the sulfide as reported by Murrell and Burnett (1986). This may be the result of our using different silicate compositions and of running at much higher T where such phases may no longer be stable. Furthermore, we did not observe the extreme variability of  $D_{\text{U}}^{\text{sulfide/silicate}}$  within a single charge that Murrell and Burnett (1986) did. This may be a function of our analyzing large areas of the sulfide that essentially averaged out heterogeneity.

This study also conflicts with the implications from Feber et al. (1984). They report Hodkin and Potter's (1980) use of arc welding to melt  $UO_2$  together with stainless steel at one atmosphere. Electron microprobe analysis showed run products with two immiscible fluids:  $UO_2$  with 1 wt% steel and steel with 23 wt%  $UO_2$ . Differences abound in experimental method and starting materials between this

study and Hodkin and Potter (1980). Unfortunately, it is not possible to resolve our different results with the information we have on hand.

Finally, observations of U's chalcophile behavior in enstatite chondrites by Furst et al. (1982), agree somewhat with the results of this study. Furst et al. contend that under highly reducing conditions, such as those found in enstatite chondrites, U partitions into CaS (oldhamite). Our data agree in that we observe some chalcophile behavior of U. However, we do not observe the same extreme U chalcophilicity. This is not unexpected due to the highly reduced character of enstatite chondrites relative to our experimental conditions. In fact, recent experiments carried out under highly reducing conditions have yielded higher U partition coefficients suggesting its possible sensitivity to oxygen fugacity (Malavergne et al., 2005; Bao et al., 2005). Oxygen fugacity in our study was constant at approximately 2 log units below IW. Consequently, we did not explore this variable.

## 6. Conclusion

The results of this study do not support the proposition that significant quantities of U partitioned into the core. For conditions relevant to the magma ocean of the early Earth, U does not significantly partition into core materials nor does it deviate from lithophile behavior. Therefore, U is unlikely to be a major contributor to the core's heat production. U does, however, display interesting chalcophile systematics with S content of sulfide and shows no variability with T and P, though these variables could be more extensively explored. It is important to note that U may behave differently at extreme conditions, such as those found at the CMB or in extremely reducing environments. Before U in the core is completely ruled out, its tendency to alloy or not with Fe at megabar-range pressures should be determined. As Th is another major source for radioactive heat in the Earth, its partitioning behavior into planetary core materials is being more thoroughly investigated.

## Acknowledgments

This research was supported by the National Science Foundation and a NASA Cosmochemistry grant. We thank E. Takahashi for providing natural KLB-1 and Nancy Chabot, Jie Li, Rick Ryerson, and Julien Siebert for their insightful and helpful reviews. We also thank Elizabeth Cottrell for technical assistance and Richard Ash for guidance on the LA-ICP-MS at the University of Maryland. LDEO contribution 6866.

Associate editor: F.J. Ryerson

## References

- Akella, J., 1973. Friction measurement in solid-media, high-pressure apparatus. *Carnegie Inst. Yearbook* **73**, 606–609.

- Bao, X., Secco, R.A., Gagnon, J.E., Fryer, B.J., 2005. Experiments of U Solubility in Earth's Core. *AGU Joint Assembl. New Orleans 2005*, # V13B-06 (abstract).
- Bertka, C.M., Fei, Y., 1997. Mineralogy of the Martian interior up to core-mantle boundary pressures. *J. Geophys. Res.* **102**, 5251–5262.
- Buffett, B.A., 2003. The Thermal State of the Earth's Core. *Science* **299**, 1675–1677.
- Bukowinski, M., 1976. The effect of pressure on the physics and chemistry of potassium. *Geophys. Res. Lett.* **3**, 491–503.
- Chabot, N.L., Agee, C.B., 2003. Core formation in the earth and moon: new experimental constraints from V, Cr, and Mn. *Geochim. Cosmochim. Acta* **67**, 2077–2091.
- Chabot, N.L., Draper, D.S., Agee, C.B., 2005. Conditions of core formation in the earth: constraints from nickel and cobalt partitioning. *Geochim. Cosmochim. Acta* **69**, 2141–2151.
- Christensen, U.R., Tilgner, A., 2004. Power requirement of the geodynamo from ohmic losses in numerical and laboratory dynamos. *Nature* **429**, 169–171.
- Cottrell, E.A., Walker, D., 2006. Constraints on Core Formation from Pt Partitioning in Mafic Silicate Liquids at High Temperatures. *Geochim. Cosmochim. Acta*, in press.
- Eggs, S.M., Rudnick, R.L., McDonough, W.F., 1998. The composition of peridotites and their minerals: a laser ablation ICP-MS study. *Earth Planet. Sci. Lett.* **154**, 53–71.
- Feber, R.C., Wallace, T.C., Libby, L.M., 1984. Uranium in the earth's core. *Eos Trans. AGU* **65**, 785.
- Furst, M.J., Stapanian, M.I., Burnett, D.S., 1982. Observation of non-lithophile behavior for U. *Geophys. Res. Lett.* **9**, 41–44.
- Govindaraju, K., 1994. Compilation of working values and sample description for 272 Geostandards. *Geostand. Newslett. Special Issue* **18**, 1–159.
- Hall, H.T., Murthy, R.V., 1971. The early chemical history of the earth: some critical elemental fractionations. *Earth Planet. Sci. Lett.* **11**, 239–244.
- Herndon, J.M., 1998. Composition of the deep interior of the earth: divergent geophysical development with fundamentally different geophysical interpretations. *Phys. Earth Planet. Inter.* **105**, 1–4.
- Herzberg, C.T., Gasparik, T., Sawamoto, H., 1990. Origin of mantle peridotite: constraints from melting experiments to 16.5 GPa. *J. Geophys. Res.* **95**, 15,779–15,803.
- Hirose, K., Kushiro, I., 1993. Partial melting of dry peridotites at high pressures: determination of compositions of melts segregated from peridotite using aggregates of diamond. *Earth Planet. Sci. Lett.* **114**, 477–489.
- Hodkin, D.J., Potter, P.E., 1980. On the chemical constitution of a molten oxide core of a fast breeder reactor. *Rev. Int. Haut. Temp.* **17**, 70–81.
- Humayun, M., Clayton, R.N., 1995. Potassium isotope cosmochemistry: genetic implications of volatile element depletion. *Geochim. Cosmochim. Acta* **59**, 2131–2148.
- Ila, P., Frey, F.A., 2000. Trace element analysis of USGS standards AGV2, BCR2, BHVO2, DTS2 and GSP2 by INAA. *J. Radioanal. Nucl. Chem.* **244**, 599–602.
- Jana, D., Walker, D., 1997. The influence of sulfur on partitioning of siderophile elements. *Geochim. Cosmochim. Acta* **61**, 5255–5277.
- Jana, D., Walker, D., 1998. Core formation in the presence of various C–H–O volatile species. *Geochim. Cosmochim. Acta* **63**, 2299–2310.
- Jones, J.H., Burnett, D.S., 2001. Laboratory studies of actinide metal-silicate fractionation, in: *Proc. 11th Lunar Planet. Sci. Conf.*, vol. 2, pp. 995–1001.
- Jones, J.H., Malvin, D.J., 1990. A nonmetal interaction model for the segregation of trace metals during solidification of Fe-Ni-S, Fe-Ni-P, and Fe-Ni-S-P Alloys. *Metall. Trans. B* **21**, 697–706.
- Kushiro, I., 1976. A new furnace assembly with a small temperature gradient in solid-media, high-pressure apparatus. *Carnegie Inst. Yearbook* **75**, 832–833.
- Labrosse, S., Poirer, J.-P., Le Mouél, J.-L., 2001. The age of the inner core. *Earth Planet. Sci. Lett.* **190**, 111–123.
- Lee, K.K.M., Jeanloz, R., 2003. High-pressure alloying of potassium and iron: radioactivity in the Earth's core. *Geophys. Res. Lett.* **30**, 2212. doi:10.1029/2003GL018515.
- Li, J., Agee, C.B., 2001. The effect of pressure, temperature, oxygen fugacity and composition on partitioning of nickel and cobalt between liquid Fe-Ni-S alloy and liquid silicate: Implications for the Earth's core formation. *Geochim. Cosmochim. Acta* **65**, 1821–1832.
- Liu, M., Fleet, M.E., 2001. Partitioning of siderophile elements (W, Mo, As, Ag, Ge, Ga, and Sn) and Si in the Fe-S system and their fractionation in iron meteorites. *Geochim. Cosmochim. Acta* **65**, 671–682.
- Malavergne, V., Tarrida, M., Combes, R., Bureau, H., 2005. Uranium and lead in the early planetary core formation: new insights given by high pressure and temperature experiments. *Lunar Planet. Sci. XXXVI*. Lunar Planet. Inst., Houston. #1823 (abstract).
- McDonough, W.F., 2003. Compositional Model for The Earth's Core. In: Carlson, R.W. (Ed.), *The Mantle and Core*. In: Holland, H.D., Turekian, K.K. (Eds.), vol. 2, *Treatise on Geochemistry*. Elsevier-Pergamon, Oxford. pp 547–568.
- Murrell, M.T., Burnett, D.S., 1982. Actinide microdistributions in the enstatite meteorites. *Geochim. Cosmochim. Acta* **46**, 2453–2460.
- Murrell, M.T., Burnett, D.S., 1986. Partitioning of K, U, and Th between sulfide and silicate liquids: implications for radioactive heating of planetary cores. *J. Geophys. Res.* **91**, 8126–8136.
- Murthy, R.V., van Westrenen, W., Fei, Y., 2003. Experimental evidence that potassium is a substantial radioactive heat source in planetary cores. *Nature* **423**, 163–165.
- Palme, H., O'Neill, H.St.C., 2003. Cosmochemical Estimates of Mantle Composition. In: Carlson, R.W. (Eds.), *The Mantle and Core*. In: Holland, H.D., Turekian, K.K. (Eds.), *Treatise on Geochemistry*, vol. 2, Elsevier-Pergamon, Oxford, pp. 1–38.
- Pearce, N.J.G., Perkins, W.T., Westgate, J.A., Gorton, M.P., Jackson, S.E., Neal, C.R., Chenery, S.P., 1997. A compilation of new and published major and trace element data for NIST SRM 610 and NIST SRM 612 glass reference materials. *Geostand. Newslett.* **21**, 115–144.
- Walker, D., Agee, C.B., 1989. Partitioning “equilibrium”, temperature gradients, and constraints on Earth differentiation. *Earth Planet. Sci. Lett.* **96**, 49–60.